Cell Reports
Physical Science

CellPress
OPEN ACCESS

Article

Molten-salt-mediated carbon dioxide capture and superequilibrium utilization with ethane oxidative dehydrogenation

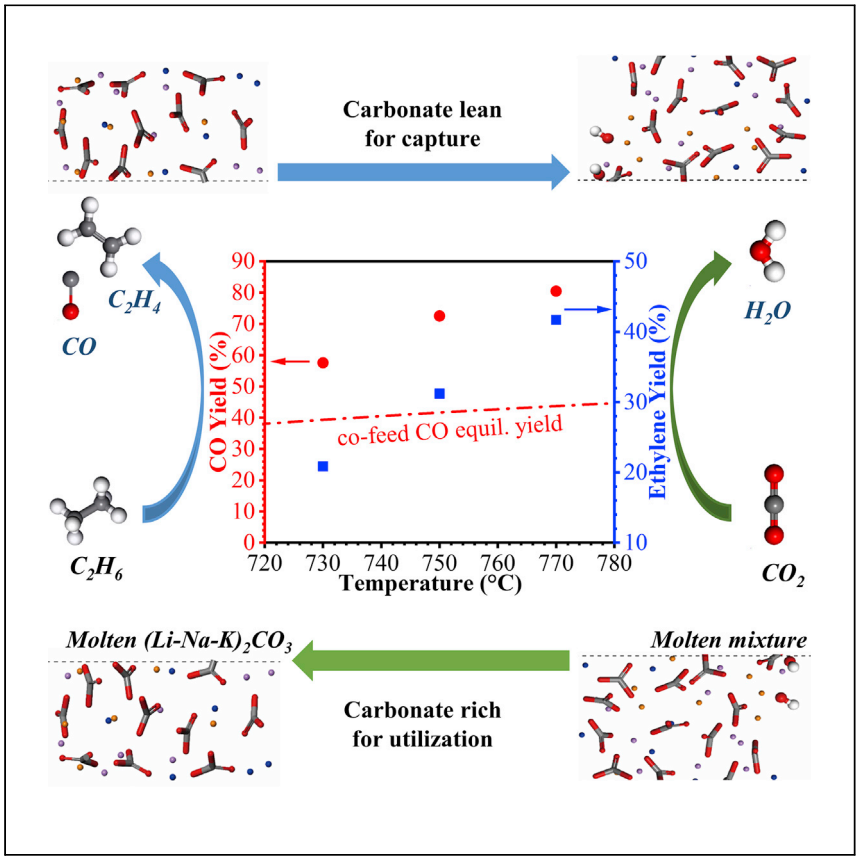

Effective CO_2 capture, sequestration, and utilization technologies in the fossil energy sector can result in significant anticipated energy savings compared to conventional approaches. Liu et al. report molten-salt-mediated ethane oxidative dehydrogenation (ODH) for integrated CO_2 capture and utilization. This approach demonstrated 89% CO_2 conversion, doubling the equilibrium of conventional CO_2-ODH. This is facilitated by partitioning CO_2-ODH into gas and molten salt phases.

Junchen Liu, Yunfei Gao, Xijun Wang, Fanxing Li

fli5@ncsu.edu

Highlights

Molten-salt reaction medium integrates CO_2 capture and utilization

89% CO yield beats equilibrium limit in CO_2 oxidative dehydrogenation of C_2H_6

Super-equilibrium CO yield realized by partitioning CO_2-ODH into separate phases

44.6% energy saved compared to conventional CO_2 capture-and-utilization approach

Liu et al., Cell Reports Physical Science 2, 100503
July 21, 2021 © 2021 The Author(s).
https://doi.org/10.1016/j.xcrp.2021.100503

Cell Reports
Physical Science

CellPress
OPEN ACCESS

Article

Molten-salt-mediated carbon dioxide capture and superequilibrium utilization with ethane oxidative dehydrogenation

Junchen Liu,[1] Yunfei Gao,[1] Xijun Wang,[1] and Fanxing Li[1,2,*]

SUMMARY

Existing CO_2-mediated oxidative dehydrogenation (CO_2-ODH) of ethane has yet to demonstrate >60% single-pass CO yield due to the intrinsic equilibrium limitations. We report a unique approach with mixed molten carbonates as a reaction medium for CO_2-ODH, which strategically partitions the CO_2-ODH reactions into gas and molten-salt phases and facilitates integrated CO_2 capture from power plant flue gases. An 89% CO yield was achieved at 770°C, doubling the equilibrium limitation of conventional CO_2-ODH. The high CO yield in turn enhances ethylene formation. Further characterizations confirmed that molten-salt mediated ODH (MM-ODH) proceeds through a gas-phase cracking and molten-salt mediated reverse water-gas-shift reaction pathway. Based on this understanding, thermodynamic analysis and *ab initio* molecular dynamics simulations were conducted to develop general principles to optimize the molten-salt reaction medium. Process analyses confirm that MM-ODH has the potential to be significantly more efficient for CO_2 capture and utilization than conventional CO_2-ODH.

INTRODUCTION

With the ever-increasing global energy consumption and rising demand for fossil fuel energy, the annual anthropogenic CO_2 emission is projected to be 45 billion tons by 2050 in a business-as-usual scenario.[1] To avoid the dire consequences of global climate change, there is an urgent need for efficient and economically viable technologies to mitigate CO_2 emissions. Although widespread utilization of renewable energy can reduce the global carbon footprint, our continued reliance on fossil fuels calls for effective CO_2 capture, sequestration, and utilization (CCSU) technologies in the fossil energy sector.

As the first step in CCSU, CO_2 capture is the most energy intensive and is responsible for 70%–80% of the total energy consumption in carbon capture and sequestration.[2–5] Rochelle[2] and others established that 220 kWh_e of energy is required to capture and compress 1 metric ton of CO_2 from coal-fired power plant flue gas, with an estimated cost of $52/ton (2009 US dollars) using well-established solvent-based technologies, such as amine scrubbing.[2] Although many alternative CO_2 capture approaches have been proposed and are in different stages of research and development, significant energy consumption and cost would nevertheless be incurred.[6–10] The energy and cost penalties associated with CO_2 capture pose significant challenges for CO_2 utilization and sequestration since they both require a concentrated CO_2 stream. Compared to sequestration, CO_2 utilization has the potential to provide significant economic incentives by converting CO_2 into valuable products.[11,12]

[1]Department of Chemical and Biomolecular Engineering, North Carolina State University, Raleigh, NC 27606, USA

[2]Lead contact

*Correspondence: fli5@ncsu.edu

https://doi.org/10.1016/j.xcrp.2021.100503

This is an open access article under the CC BY-NC-ND license (http://creativecommons.org/licenses/by-nc-nd/4.0/).

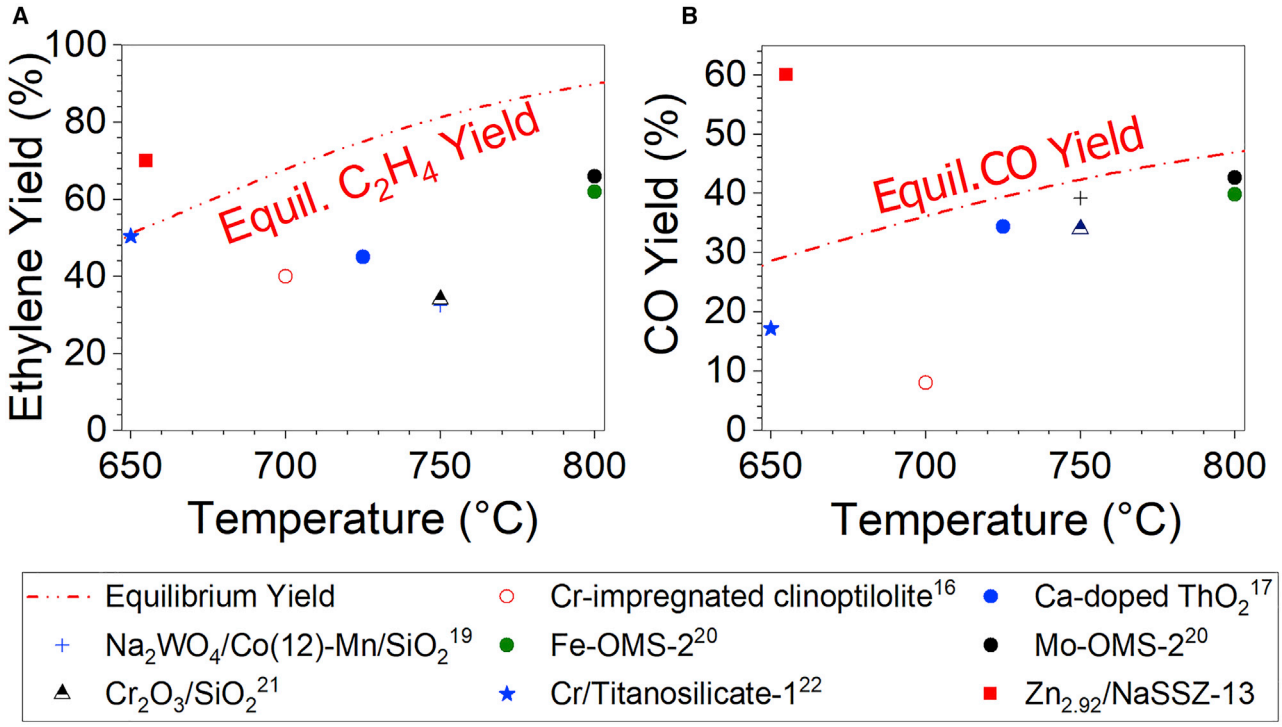

Figure 1. Equilibrium (CO_2/C_2H_6 = 1) and experimentally obtained yields of selected ethane CO_2-ODH catalysts.
(A) C_2H_4 yields.
(B) CO yields.

CO_2 utilization technologies investigated to date include CO_2 to fuel, CO_2 to chemicals, and CO_2 enhanced oil recovery.[11–15] Among these, CO_2-mediated oxidative dehydrogenation (CO_2-ODH) of light alkanes, particularly ethane,[14,16–24] has opened up new and exciting opportunities for (1) producing a value-added ethylene product, which is in high demand and energy intensive to produce[25]; (2) simultaneous utilization of the abundantly available ethane resulted from the shale gas revolution[26]; and (3) co-production of CO, a valuable industrial gas.

Ethane is the largest wet (C_{2+}) component in shale gas and represents, on average, 24 vol% of the gas produced in Bakken.[27] The surge in ethane supply and the energy intensity in conventional ethane conversion processes call for efficient and low-emission approaches to convert ethane to ethylene.[28] Ethylene yield in commercial steam cracking processes is equilibrium limited due to the formation of H_2 as a coproduct. As such, the single-pass ethylene yield is generally limited to ~55% in steam crackers. To address this challenge, oxidative ethane dehydrogenation using CO_2 as a soft oxidant (CO_2-ODH) was widely investigated. Two primary reaction pathways for CO_2-ODH that have been reported include (1) direct ethane cracking reaction followed by a reverse water-gas shift (RWGS) reaction to convert the by-product H_2 into CO and H_2O,[14] as described in Reactions 1 and 2, and (2) catalytic oxidative dehydrogenation of ethane with CO_2, typically on a metal oxide catalyst surface through a Mars-van Krevelen type mechanism.[14] In either reaction pathway, the overall reaction can be written as Reaction 3. Figure 1 summarizes the equilibrium ethylene and CO yield in CO_2-ODH based on a C_2H_6/CO_2 = 1/1 molar-flow based feed condition. We note that by-products such as $C3_+$, coke, and steam reforming products are not included in the equilibrium analysis since they are kinetically limited in the context of ethane cracking conditions. We further note that the

deviation of the carbon balance of our experiments are within ±7%. Furthermore, we determined via H_2 balance that the dry reforming activity contributed ≤0.7% to the CO yield in all cases. This represents a commonly accepted approach to analyze ethane cracking reactions.[29–33]

$$C_2H_6 \leftrightarrow C_2H_4 + H_2 \quad \text{(Reaction 1)}$$

$$CO_2 + H_2 \leftrightarrow CO + H_2O \quad \text{(Reaction 2)}$$

$$CO_2 + C_2H_6 \leftrightarrow CO + C_2H_4 + H_2O \quad \text{(Reaction 3)}$$

To date, most CO_2-ODH studies focus on catalyst development with the goal of improving ethylene selectivity and yield. Numerous high-performance catalysts have been reported, along with important mechanistic insights, warranting further investigation of this important subject.[13–16,18–21,23,24,34] Although single-pass ethylene yields reported on a number of CO_2-ODH catalysts (Figure 1A) were comparable to those in commercial steam ethane cracking (~55%), CO yields $\left(Y_{CO} = \frac{y_{CO}}{y_{CO} + y_{CO_2}}\right)$ still remained severely equilibrium limited (Figure 1B). Using a catalyst composed of highly dispersed zinc on Na-SSZ-13 zeolite, a CO yield up to 60% along with 70% ethylene yield was achieved at 650°C, using diluted (5 vol%) C_2H_6 and an equal part of CO_2.[35] Another, earlier study reported a CO yield of 55.7% at 830°C for a K-Cr-Mn-O/SiO_2 catalyst, but this relatively high CO yield resulted from severe coking and dry reforming activities, which sacrificed the ethylene selectivity.[24] Other promising CO_2-ODH catalysts include those containing Cr and/or Ni. Their CO_2 conversions are generally lower than 45%, but with satisfactory ethylene selectivity (>80%) and reasonable coke resistance.[19,21,36–40] While CO_2 conversion (or CO yield) has received little attention in most of the previous CO_2-ODH studies, it is an important parameter to consider since (1) gaseous products from ethane ODH need to undergo compression and deep cooling before cryogenic distillation; a low CO_2-to-CO conversion would significantly increase the cost and energy consumption in these stages due to the presence of H_2, negatively affecting the attractiveness of CO_2-ODH[25]; and (2) the increase in the yield of CO, a high-value product, can increase the overall product value while promoting the effectiveness for CO_2 utilization. Given that both RWGS and CO_2-ODH of ethane reactions are endothermic, CO_2-ODH is favored at higher temperatures from a thermodynamic standpoint. Nonetheless, the CO yield of the experimental studies reported to date are generally limited to ~45%, even when carried out at 800°C, as shown in Figure 1. This is understandable given the intrinsic thermodynamic limitations on CO_2 conversion, which in turn limits the maximum ethylene yields. Another important challenge to conventional CO_2-ODH resides in the needs for purified CO_2, which is energy intensive to capture and separate. To summarize, an ideal CO_2-ODH technology should be able to (1) combine CO_2 capture and utilization into an integrated process and (2) achieve high CO and ethylene yields without being subjected to the equilibrium limitations witnessed in conventional approaches.

Integration of carbon capture and utilization has been attempted in the context of dry reforming of methane. Both Tian et al.[41] and Buelens et al.[42] used a hybrid system involving a calcium oxide-based sorbent and Ni-based catalysts to capture CO_2 followed by converting carbonate formed into CO and/or H_2. The high operating temperature and relatively low methane feed concentration alleviate equilibrium limitations for dry (or "super dry") reforming, allowing high CO/H_2 yields. To the best of our knowledge, integration of CO_2 capture and utilization for ethylene

production in an isothermal system have only been reported by Al-Mamoori et al.[43] In their study, an H-Zeolite Socony Mobil 5 (H-ZSM-5)-based dehydrogenation catalyst layer is used in conjunction with a K_2O-CaO, Na_2O-CaO, and CaO-based CO_2 sorbent layer in a packed bed reactor. Captured CO_2 is released from the sorbent by raising the reactor temperature in the ethane conversion step. A 22% ethylene yield was reported, along with 14% CO_2 conversion due largely to the aforementioned equilibrium limitations. In principle, a hybrid system involving a CO_2 sorbent and heterogeneous catalyst could be used for CO_2-ODH of ethane. However, more severe equilibrium limitations would be anticipated, considering the high endothermicity for carbonate decomposition during the CO_2 utilization/ethane conversion step.[44–46]

Here, we proposed and demonstrated a molten-carbonate-mediated ODH (MM-ODH) approach to capture and use CO_2 for the co-production of ethylene and CO with high yields. The strategic design of the molten-carbonate system circumvents the equilibrium limitations imposed on conventional CO_2-ODH processes, achieving a super-equilibrium CO yield of 89.2%, doubling the equilibrium yield for conventional CO_2-ODH. This novel process also attained 93% ethylene selectivity, with 98% total olefin selectivity and 56% H_2 conversion. In the following sections, an overview of the MM-ODH process and the rationale behind the equilibrium circumvention using molten-salt as both a reaction and CO_2 capture medium are discussed first. Subsequently, the feasibility of the process is experimentally validated. An investigation of the reaction pathway is then presented, as well as thermodynamic analyses to examine the selection of the molten-salt reaction media. Finally, an energy analysis is presented to determine the process efficiency for CO_2 utilization.

RESULTS AND DISCUSSION

MM-ODH reaction scheme and proof of concept

As illustrated in Figure 1, CO yield with the simultaneous presence of CO_2 and ethane is equilibrium limited irrespective of the ODH catalyst type. Such an equilibrium limitation would be even more severe if a solid CO_2 sorbent was used. For instance, integrating $CaCO_3$ as the source of CO_2 in ODH would make the CO_2-ODH process 167.6 kJ/mol more endothermic at 800°C and limit the CO_2 conversion to 41% (versus 47% with CO_2 co-feed), as calculated by HSC Chemistry Outotec version 10. This additional thermodynamic limitation would appear to be inevitable for any CO_2-ODH approach with integrated CO_2 capture since a system that is spontaneous for CO_2 capture would have a natural tendency to inhibit CO_2 release, adding the difficulty for CO_2 conversion in CO_2-ODH from a thermodynamic standpoint. To circumvent this challenge, we propose to use molten carbonates as a reaction medium to partition the CO_2 and ethane in the liquid phase and the gas phase, respectively. Unlike solid CO_2 sorbents, which have a fixed activity coefficient of 1 for the gas phase CO_2-ODH reactions, the molten carbonate system enables simultaneous equilibria in both gas and liquid phases, as illustrated in Figure 2A. As discussed here through the detailed thermodynamic analyses in later sections, the eutectic formation can increase the activity of the molten carbonate salt, allowing "super-equilibrium" CO yields. A schematic of the MM-ODH approach based on the above-mentioned strategy is shown in Figure 2B. As illustrated, MM-ODH integrates CO_2 capture and ethane CO_2-ODH into the molten carbonate reaction medium. The MM-ODH system is operated in two cyclic steps, forming a reaction loop: in step 1, molten carbonates are converted into CO and hydroxides by H_2 generated from ethane dehydrogenation; in step 2, the molten hydroxides subsequently capture CO_2 from a flue gas stream while regenerating the carbonates.

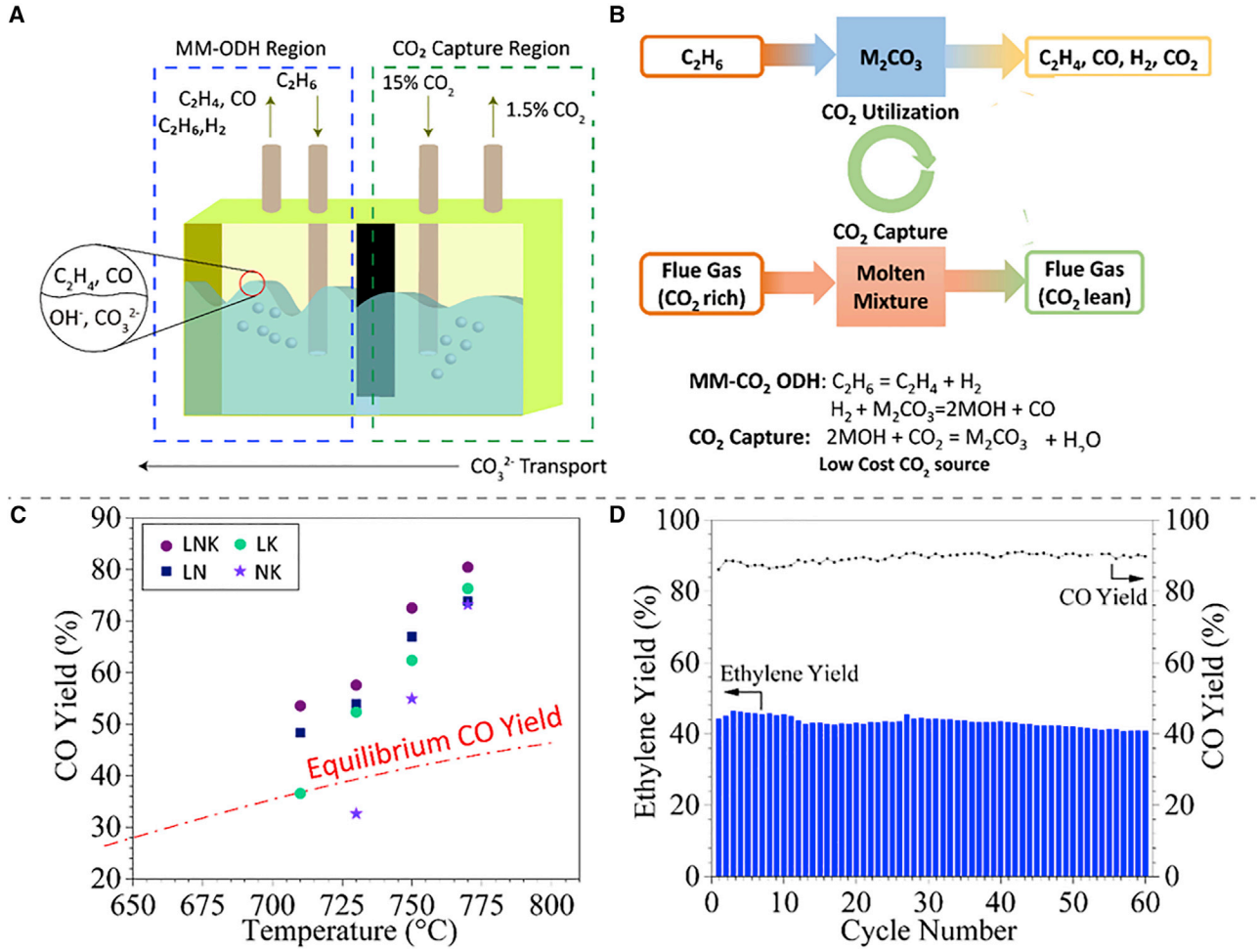

Figure 2. MM-ODH scheme and CO_2 utilization performance

(A) A conceptual reactor schematic with molten carbonate reaction media designed to simultaneously capture CO_2 and convert ethane.

(B) Simplified schematic of the MM-ODH process.

(C) MM-ODH reaction results for LNK, $(Li\text{-}Na)_2CO_3$ (LN), $(Li\text{-}K)_2CO_3$ (LK), and $(Na\text{-}K)_2CO_3$ (NK) at different temperatures.

(D) Performance of 60 cycle tests with LNK at 770°C.

Figures 2C and 2D highlight our experimental results, under an integral basis, demonstrating the feasibility and attractiveness of MM-ODH. These results were obtained with $(Li\text{-}Na)_2CO_3$, $(Li\text{-}K)_2CO_3$, $(Na\text{-}K)_2CO_3$ (NK), and $(Li\text{-}Na\text{-}K)_2CO_3$ (LNK) salt mixtures at their respective eutectic compositions and tested in a 1-in outer diameter (OD) alumina tube. The selection of the carbonate mixtures is based on the melting point and its stability (i.e., lower CO_2 release). NK is not included at 710°C due to its high melting point of 710°C.[47] In addition, the high melting point of Li_2CO_3 (724°C) makes it unsuitable for experimental investigation. The experimental setup and method of calculation are described in Notes 4.1 and 4.2, Figure S1, and Table S1. As can be seen in Figure 2C, MM-ODH exhibited significantly higher CO yields than those predicted from conventional CO_2-ODH equilibrium. For all of the molten-salts screened, the CO yields increased with temperature. At 770°C, all molten salts demonstrated CO yields $\geq$73%. A maximum CO yield of 89.2% was achieved with LNK mixed molten-salts, nearly doubling the equilibrium CO yield in conventional CO_2-ODH. In the extended ODH step, the CO yields could reach up to 92.2% at 770°C, as shown in Figure S2. The LNK molten salts also

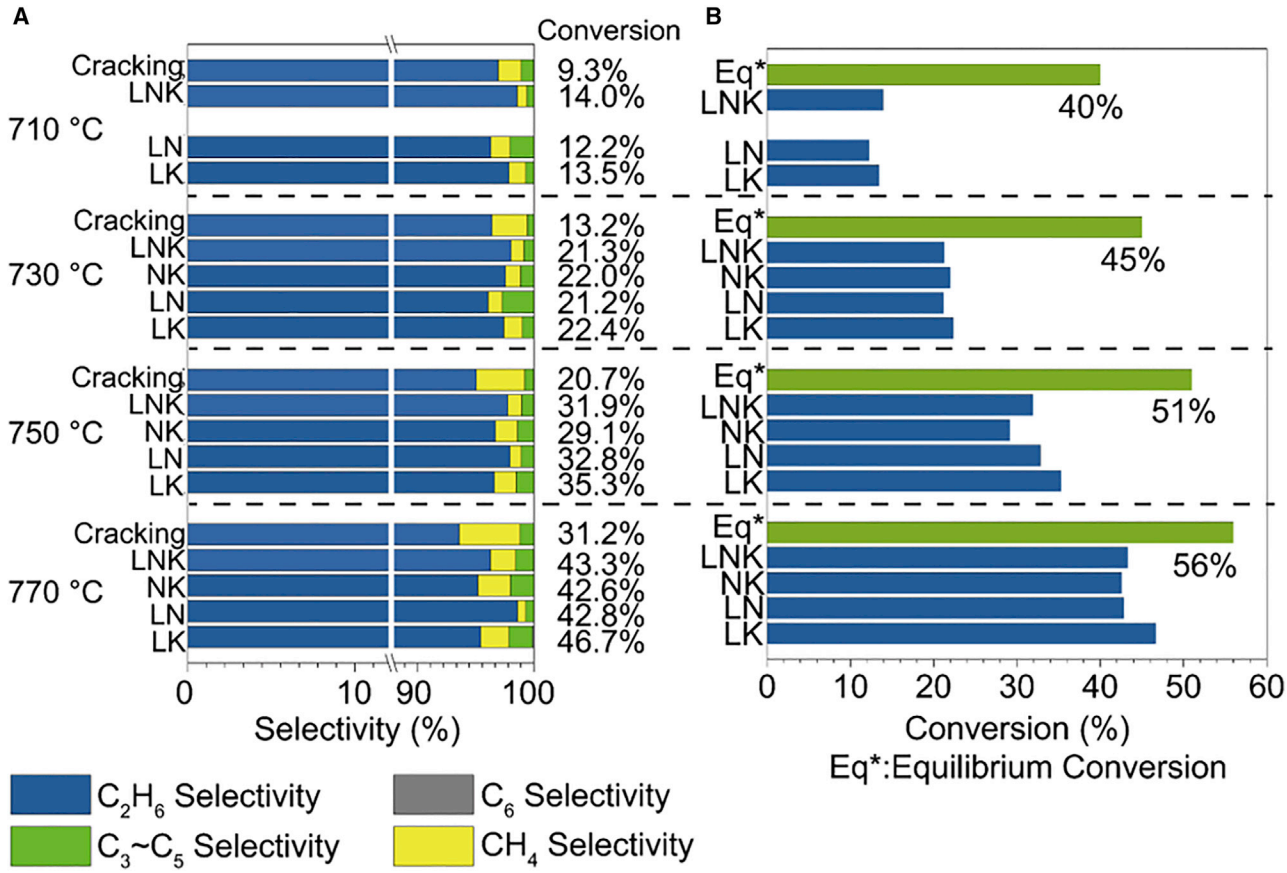

Figure 3. Ethane conversion performance of MM-ODH

(A) MM-ODH results with LNK, NK, LN, and LK reaction media. Thermal (blank) cracking results are shown for comparison purposes. Reaction conditions: 10 vol% ethane (balance Ar), 50 mL/min total gas flow rate.

(B) Conversion profiles for MM-ODH in comparison with equilibrium conversion of CO_2-ODH of ethane.

exhibited a stable ethylene yield averaging 43.4% and a CO yield averaging 89.4% for >60 cycles (Figure 2D). In addition, the contribution of reforming activity and coke formation are limited to $\leq$0.7% at 770°C, as determined by the hydrogen and CO balance described in Equation S1. We note that our definition of CO yield can also be interpreted as CO_2 conversion, since CO is the only product resulting from CO_2 conversion and the contribution of CO from dry reforming is negligible.

MM-ODH also demonstrated higher ethylene yields when compared to thermal cracking of ethane. As shown in Figures 3A and 3B, each molten-salt eutectic system exhibited selectivity to ethylene above (>90%) at 770°C and ethane conversion above 70%, with a slightly higher selectivity in C_3–C_5 and methane than that of thermal cracking. The formation of C_{6+} species are negligible in all cases. As one would anticipate, the ethylene selectivity decreased with increasing temperature, while ethane conversion and olefin yields increased. Methane, C_4, and C_{6+} accounted for $\leq$5% of the overall product selectivity.

The CO_2 capture and storage capability of the molten-salts was further examined through thermogravimetric analysis, with results shown in Figures S3 and S4. To further confirm the ability of the molten-salt to capture diluted CO_2 in a flue gas stream, 3 vol% CO_2 was flowed through fully decomposed Li_2CO_3, the alkali metal

carbonate with highest tendency to decompose into CO_2 and oxide. As shown in Figure S3, the sorbent is highly reactive toward this dilute CO_2 stream at CO_2 concentrations well beneath the typical flue gases concentration (~12–15 vol%). The CO_2 capacity of the molten-salt sorbent was stable under repeated cycles (Figure S4). In comparison, the $CaCO_3$ sorbent-based CO_2 capture system tends to experience significant sintering-induced deactivation within 20 carbonation-calcination cycles.[48–57] Although few recent studies have resulted in rather sintering-resistant calcium sorbents, precise morphological controls are required.[48–57] These results demonstrate that the MM-ODH can be a promising process for CO_2 capture and utilization in the context of ethane ODH.

MM-ODH reaction pathway

The notably higher ethylene yields compared to thermal cracking may be explained by one of the two possible mechanisms: (1) a kinetically driven yield increase (i.e., the molten carbonate reaction medium acts as a "catalyst" to accelerate the ethane dehydrogenation reaction) or (2) a thermodynamically driven yield increase (i.e., the consumption of the H_2 through CO_2 conversion, which decreases the reverse reaction rate for MM-ODH). To probe the possible mechanism of the reactions, a temperature-programmed reaction was carried out to determine the kinetic contribution, followed by *in situ* diffuse reflectance infrared Fourier transform spectroscopy (DRIFTS) and H_2/CO_2 cofeed experiment to establish the roles of carbonate and hydroxide in the reaction system.

A temperature-programmed reaction (TPR) was carried out to determine whether the molten-salt would contribute to the activation of ethane. A relatively high gas hourly space velocity (GHSV) (1,200 h^{-1}) was used to ensure that the system is operated under a kinetic regime with minimal thermodynamic effects. It was determined that the onset temperature for ethane dehydrogenation was higher in the presence of the molten-salt than that with ethane thermal cracking alone (Figure S5). The ethylene yield in the molten carbonate system was notably lower than that of the ethane cracking in this kinetic regime, thus ruling out the catalytic effect of the molten carbonates system toward ethane conversion. The improved ethylene yields relative to thermal cracking (Figure 2) are therefore thermodynamically driven due to H_2 consumption by a RWGS reaction.

To further understand the role of the molten phase in RWGS reactions, the experimental results of CO_2/H_2 cofeed in an empty tube versus H_2 feed to molten LNK were compared. The presence of the molten salt increased CO yield by >6-fold, from 14% to 92% (Table S2). The significant enhancement in the CO yield primarily resulted from the fixation of CO_2 in the molten phase. Meanwhile, H_2 conversion was increased from 21% to 29%. These results clearly supported that the molten-salt acts as a reaction medium for H_2 conversion reaction in a molten-salt-mediated RWGS (MM-RWGS) reaction and it was a primary contributor to higher CO yields. These results also suggest that the super-equilibrium CO yield resulted from partitioning CO_2 in the liquid phase and C_2H_6 in the gas phase. By fixating CO_2 in the molten-salt, the H_2 conversion increased and the CO_2 in the product gas would be significantly lower.

The participation of the molten carbonate in the MM-RWGS reaction was further verified by *in situ* DRIFTS under isothermal H_2/CO_2 cycles with LNK. Due to the limitation of the instrument, the study was performed at 600°C. While few species could adsorb on the surface at high temperatures, we note that at 600°C, the LNK is in a liquid phase, and the purpose of DRIFTS was to detect species in the liquid phase.

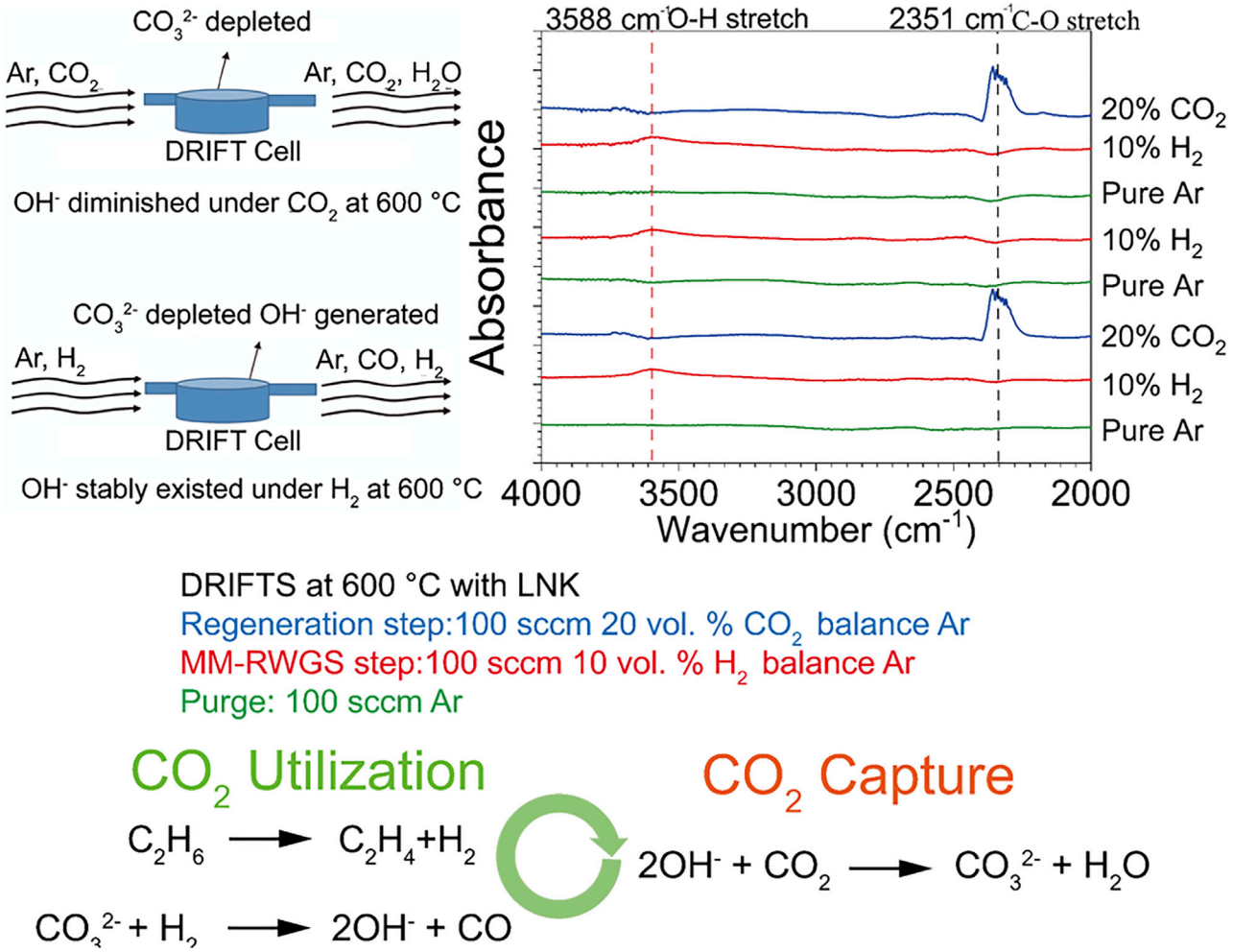

Figure 4. *In situ* DRIFTS experiments

600°C on MM-ODH reactions in the presence of a Li_2CO_3, Na_2CO_3, and K_2CO_3 eutectic reaction medium.

As shown in Figure 4, the injection of H_2 (10%, balance Ar) resulted in a peak at 3,588 cm^{-1}, assigned to the O-H stretching, indicating that OH^- was formed when CO_3^{2-} was exposed to H_2 via a molten-salt-mediated RWGS reaction, as shown in Reaction 4 using Li_2CO_3 as an example:

$$Li_2CO_3 + H_2 \leftrightarrow 2LiOH + CO \quad \text{(Reaction 4)}$$

We note that although for Reaction 4, $\Delta G > 0$, it still proceeded to produce significant amounts of CO and LiOH since carbonate was in large excess.

Figure 4 further indicated that the O-H stretching peak disappeared under 20% CO_2 and the C-O stretch peak characteristics of CO_3^{2-} appeared. This indicated that CO_2 was captured by the molten-salt and OH^- was converted back to CO_3^{2-}. These findings were further verified in Figure S6. It can be concluded that the role of the carbonate include (1) uplifting the RWGS equilibrium limitation by partitioning the reaction between the gas and molten-salt phases and (2) integrating the CO_2 capture.

To summarize, the MM-ODH reaction proceeds through a parallel gas-phase cracking and molten-salt-mediated RWGS reaction pathway. That is, the presence of the molten

carbonates facilitate hydrogen conversion into CO and (molten) hydroxides, which increase the ethylene yield. *In situ* conversion of H_2 in turn enhances ethane cracking by alleviating equilibrium limitations. The alkali metal hydroxides formed in the ODH step are highly effective for CO_2 capture to regenerate the carbonates, enabling a cyclic CO_2 capture-and-utilization scheme. The thermodynamic feasibility and the criteria for molten salt selection are discussed further in the next section.

Thermodynamic analysis and effect of molten-salt compositions

Given that ethane conversion in MM-ODH is thermodynamically driven, and that the high CO_2 conversion resulted from partitioning the reactions in both the gas and liquid phases, it would be informative to determine the effect of molten-salt compositions on the reaction thermodynamics. Due to the complexity of the MM-ODH reaction system, a hybrid thermodynamic analysis method combining HSC Chemistry software and numerical thermodynamic analysis was used. HSC Chemistry was used to establish the equilibrium among H_2, CO_3^{2-}, OH^-, H_2O, CO_2, CO, O^{2-} between 500°C and 900°C. The result was combined with the thermal cracking equilibrium constant obtained via HSC Chemistry to determine the equilibrium yield of ethylene. The ethane-reforming reaction, which was observed to be negligible in experiments, was not considered in the analysis.

The activities of all of the eutectics tested in the experiments were calculated by adopting the Temkin equation to account for the deviation from the ideal solution assumption, as shown in Equations S2–S5. The results from these analyses, summarized in Figure 5, demonstrate that the experimental ethylene and CO yields were both below the thermodynamic limits in the two-phase system. This confirmed that while the MM-ODH process circumvents the conventional CO_2-ODH equilibrium by partitioning the liquid gas phase product and alternating reaction route, the reactions themselves do not violate the thermodynamic limit in the MM CO_2-ODH system.

During the ODH step, the molten-salt primarily functions as a reaction medium to facilitate a modified RWGS with carbonate ions in the liquid phase. The extent of this modified RWGS reaction, which is directly related to the tendency of the carbonate for decomposition, would (1) affect H_2 conversion, which in turn affects the ethylene yield by shifting the ethane pyrolysis equilibrium, and (2) affect the CO yield. Figure 5A illustrates the equilibrium CO_2 partial pressures ($P_{CO_{2,eq}}$) for the carbonates of interest. Li_2CO_3, which had the greatest tendency to decompose into Li_2O and CO_2, had the highest equilibrium partial pressure. Given that Na_2CO_3 and K_2CO_3 were more stable than Li_2CO_3, mixing Li_2CO_3 with Na_2CO_3 or K_2CO_3 decreased the $P_{CO_{2,eq}}$. NK being the eutectic of Na_2CO_3 and K_2CO_3, as anticipated, has the lowest $P_{CO_{2,eq}}$. As can be expected, a low $P_{CO_{2,eq}}$ would generally lead to high CO yield (Figures 5A and 5B), since minimal CO_2 would be produced during the ODH step. However, $P_{CO_{2,eq}}$ being too low would lead to low equilibrium conversion of the modified RWGS reaction and, hence, low H_2 conversion (Figure 5C). A low H_2 conversion would in turn lead to low ethylene yield (Figure 5D). An intermediate $P_{CO_{2,eq}}$ can thus enhance both CO yield (a combination of low CO_2 slippage and high carbonate conversion) and high ethylene yield. From Figure 5, it can be concluded that LK provides a satisfactory balance among CO yield, H_2 conversion, and ethylene yield. LNK is not included in Figure 5 since the correlation for its activity coefficient is not available, but Janz[58] had shown that the $P_{CO_{2,eq}}$ of LNK was comparable to other binary eutectic, as shown in Table S3. The Gibbs free energies calculated from *ab initio* molecular dynamics (AIMD) simulations further corroborated this analysis, as can be seen in Figure 6 (see Note S4 for more details). The estimated reaction Gibbs free energy (ΔG) of LK is 0.74 eV (71.40 kJ/mol) higher than that of

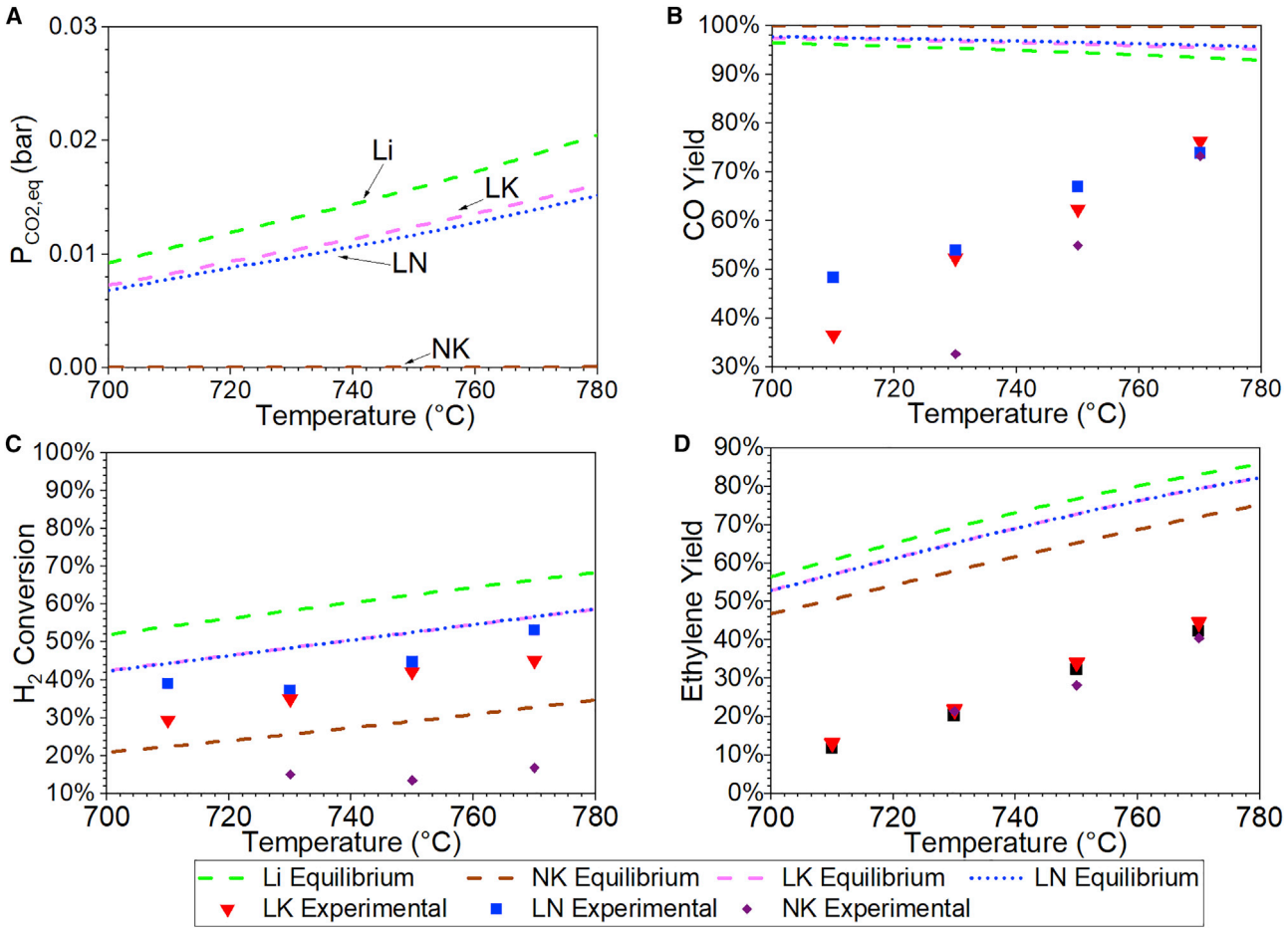

Figure 5. Thermodynamic analysis of MM-ODH systems

(A) Equilibrium CO_2 partial pressure.

(B) Equilibrium CO yield.

(C) Equilibrium H_2 conversion.

(D) Equilibrium ethylene yield of Li_2CO_3 (Li), 62%Li_2CO_3-38%K_2CO_3 (LK), 55%Li_2CO_3-45%Na_2CO_3 (LN), 43.5%Li_2CO_3-31.5%Na_2CO_3-25%K_2CO_3 (LNK) at the molar ratio used in experiments. The symbols correspond to the experimental results. Li_2CO_3 was not investigated experimentally due to the high melting point.

Li_2CO_3 in terms of the modified RWGS, which would lead to a lower equilibrium conversion of modified RWGS for LK than that of Li_2CO_3. However, in terms of carbonation reaction, since the ΔG of LK is 0.78 eV (75.26 kJ/mol) lower than Li_2CO_3, the $P_{CO_{2,eq}}$ of LK would be significantly lower than that of Li_2CO_3, indicating a significantly higher CO yield. Since the ΔG of LNK on modified RWGS and carbonation reaction are between Li_2CO_3 and LK, and that the ΔG of the carbonation reaction is negative, an intermediate equilibrium conversion of modified RWGS and a low $P_{CO_{2,eq}}$ is expected for LNK. As shown in Figures 2 and 3, LNK exhibits its potential for desirable CO yield, H_2 conversion, and ethylene yield. Furthermore, our experiments indicated that LNK has the potential for a high H_2 conversion, as shown in Table S4, supporting the idea that this ternary eutectic could be an optimal choice for MM-ODH from a thermodynamic standpoint.

Energy consumption for CO_2 utilization

With the feasibility of MM-ODH validated by both thermodynamic analysis and experimental data, it would be desirable to compare its energy requirement when

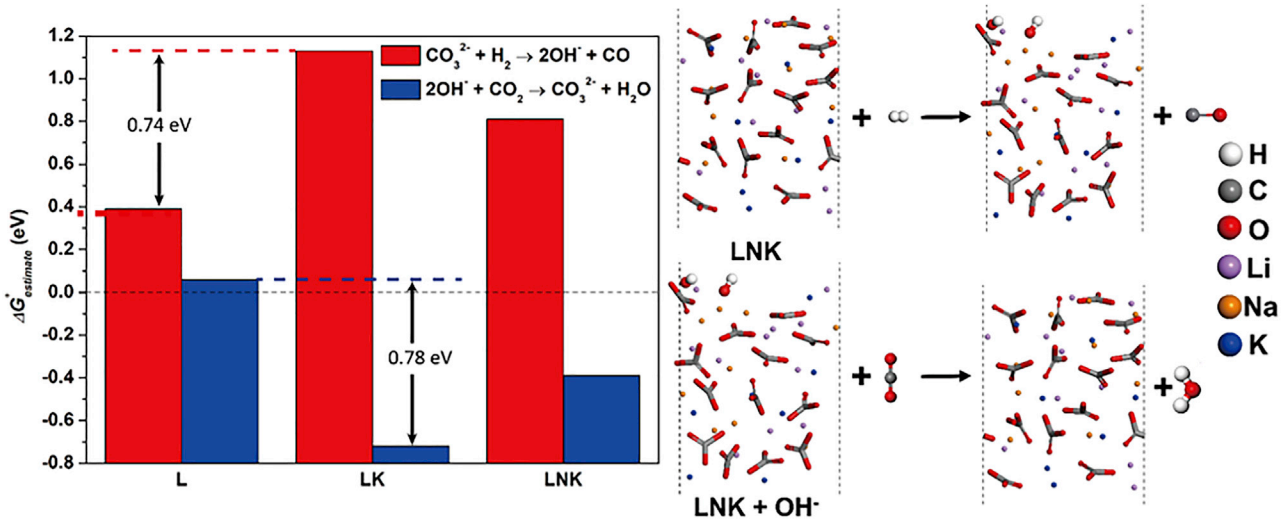

Figure 6. *Ab initio* molecular dynamic results
Gibbs free energy of modified RWGS and carbonation reaction of L, LK, and LNK.

compared to the conventional CO_2-ODH. ASPEN Plus simulation was used to model the energy requirements for both MM-ODH and conventional CO_2-ODH. Both models were detailed in Figures S8–S10, Tables S6–S12, and Note S3. For CO_2-ODH, OMS-2 catalyst was selected for modeling purposes, because it demonstrated the highest ethylene and CO yields based on reports in the literature and was operated at a higher temperature than MM-ODH.[20] Figure 7A demonstrated key energy requirements for the process. Unlike CO_2-ODH, the regenerator that was used to capture CO_2 was a net exothermic reaction that offset 52.5% of the heat required from the MM-ODH reactor. The CO_2 lean stream was then used for heat integration and stream generation. Consequently, the upstream energy requirement was significantly reduced. The main energy savings in the downstream was from a 91.5% lower energy requirement for amine scrubbing. Other energy savings such as lower compression and refrigeration duty was due to higher CO_2 conversion and lower moles flow on a dry basis. Energy savings were also observed from methane distillation due to a 50% decrease in CH_4 selectivity and CO purification due to higher H_2 conversion and minimum coking activity in the MM-ODH case. Overall, MM-ODH can lead to a 31.9% energy reduction when compared to CO_2-ODH with OMS-2 to capture and convert 1 metric ton of CO_2. We also note that both processes co-produce C_2H_4 and H_2 along with CO. To more accurately quantify the energy consumed for CO_2 capture and conversion (to CO), the energy associated with ethylene and H_2 production are subtracted from the overall process energy consumption, as illustrated in Figure 7B. Corresponding assumptions and calculations are given in the supplemental information.[25,59] As can be seen, the energy consumption for CO_2 capture and utilization was 8.8 GJ/ton CO_2 for MM-ODH and 15.9 GJ/ton CO_2 for CO_2-ODH with OMS-2. This corresponds to a 44.6% energy reduction from the proposed MM-ODH approach.

The present study reports alkali metal carbonates as effective reaction media for CO_2-ODH of ethane with integrated CO_2 capture. This molten-salt-mediated ODH (MM-ODH) process demonstrated a CO yield up to 89.2%, nearly doubling the equilibrium CO yield in conventional CO_2-ODH processes. In addition, an equilibrium-enhanced ethylene yield with 93% ethylene selectivity and >98% olefin selectivity was demonstrated. The super-equilibrium CO yield was achieved by

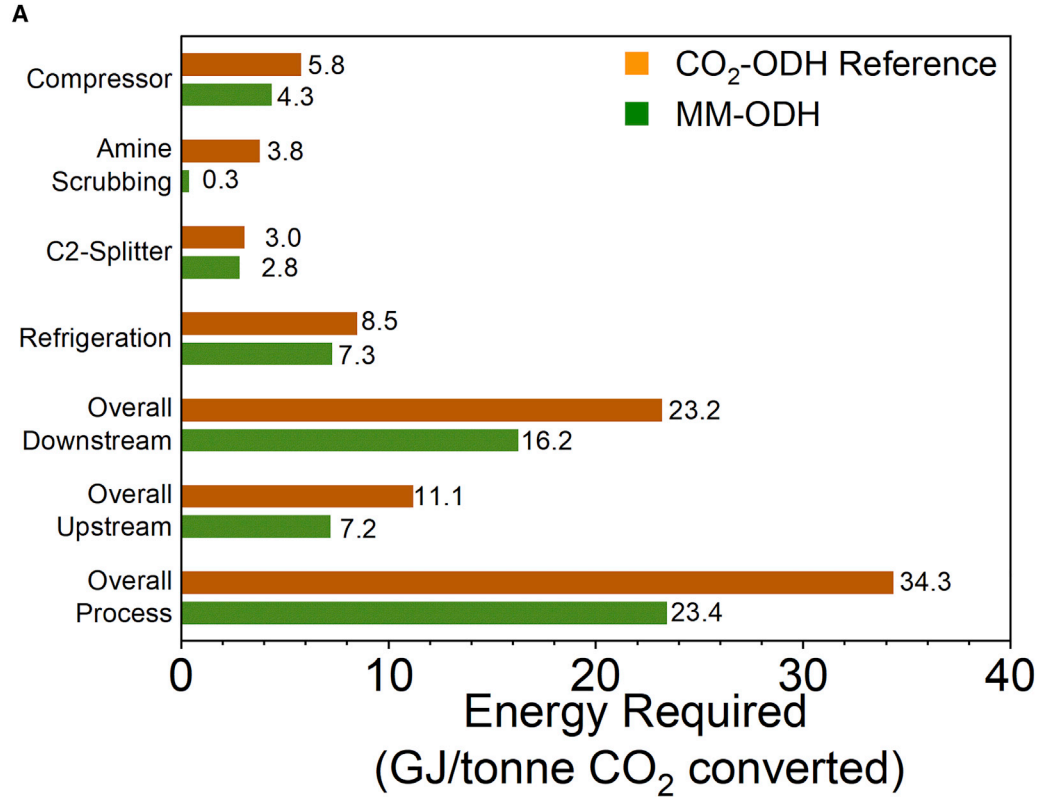
A
Compressor
Amine Scrubbing
C2-Splitter
Refrigeration
Overall Downstream
Overall Upstream
Overall Process
5.8
4.3
3.8
0.3
3.0
2.8
8.5
7.3
23.2
16.2
11.1
7.2
34.3
23.4
CO2-ODH Reference
MM-ODH
0
10
20
30
40
Energy Required
(GJ/tonne CO2 converted)

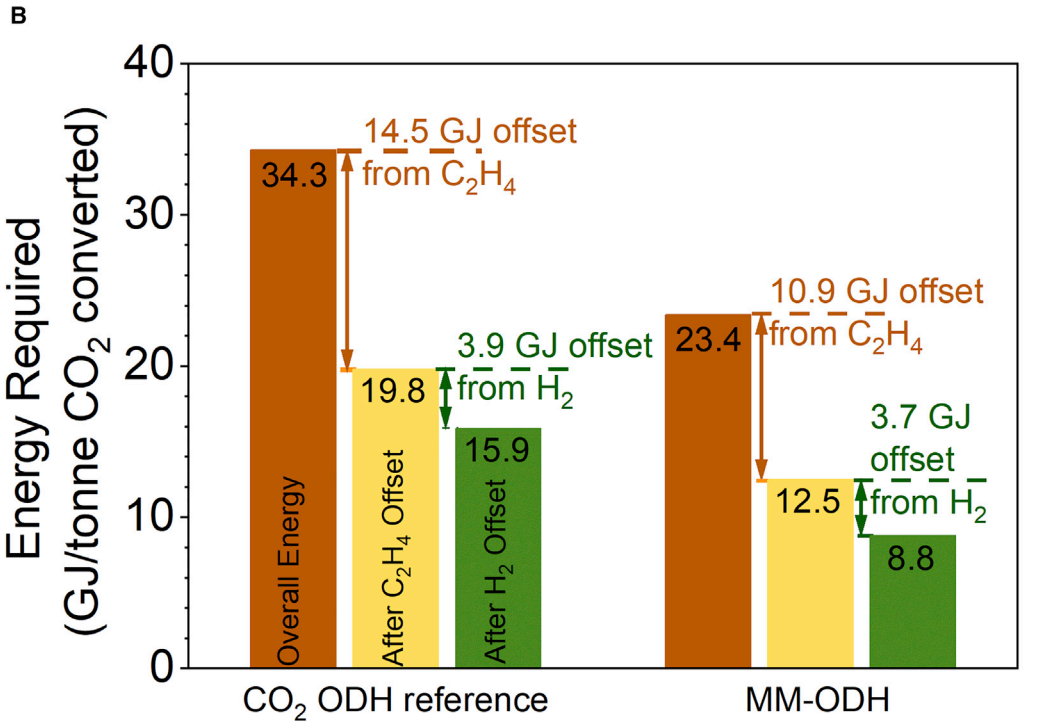
B
Energy Required
(GJ/tonne CO2 converted)
0
10
20
30
40
34.3
14.5 GJ offset
from C2H4
19.8
3.9 GJ offset
from H2
15.9
Overall Energy
After C2H4 Offset
After H2 Offset
23.4
10.9 GJ offset
from C2H4
12.5
3.7 GJ
offset
from H2
8.8
CO2 ODH reference
MM-ODH

partitioning the CO_2-ODH reactions into both gas and molten-salt phases, as confirmed by a detailed thermodynamic analysis. The analysis was also shown to be effective to project the relative performance of the various molten-salt reaction media. Characterizations of the MM-ODH reactions indicated that ethane conversion in the presence of molten carbonate reaction media proceeds through a parallel gas-phase cracking and molten-salt-mediated RWGS reaction. The presence of the molten carbonates facilitates hydrogen conversion into CO and molten hydroxides via a MM-RWGS reaction. *In situ* conversion of H_2 in turn enhances ethane cracking by alleviating equilibrium limitations. The alkali metal hydroxides formed in the ODH step are highly effective for CO_2 capture to regenerate the carbonates, enabling stable performance for cyclic CO_2 capture followed by CO_2 utilization via ethane ODH. ASPEN Plus simulation indicates that the MM-ODH approach can result in up to a 44.6% energy savings for integrated CO_2 capture and utilization.

EXPERIMENTAL PROCEDURES

Resource availability

Lead contact

Further information and requests for resources and reagents should be directed to and will be fulfilled by the lead contact, Dr. Fanxing Li (fli5@ncsu.edu).

Materials availability

This study did not generate new unique reagents.

Data and code availability

The authors declare that data supporting the findings of this study are available within the article and the supplemental information. All other data are available from the lead contact upon reasonable request.

Carbonate eutectics synthesis

The carbonate eutectics were synthesized according to the literature.[60] The carbonate eutectics was synthesized with Li_2CO_3 (99.9%, Sigma-Aldrich), Na_2CO_3 (99.9%, Sigma-Aldrich), K_2CO_3 (99.9%, Sigma-Aldrich) at the given compositions. The compositions were further elucidated in Note S1.1.

Fixed-bed experiment

The fixed-bed experiment is demonstrated in Figure S1A. The MM-ODH process was carried out in an alumina tube (99.9%, McDanel) with an inner diameter (ID) of 1 in under a fixed bed mode. In each experiment, 10 g of the well-mixed eutectics were loaded into the tube and were externally heated with a furnace with a K-type thermocouple to measure the temperature of the furnace. A gas-mixing panel with multiple Alicat mass flow controllers (MFCs) was used to deliver the gaseous mixture. The furnace was heated up to the desired temperature (710°C–770°C) at a rate of 20°C/min. After the mixture was melted above its melting point, a $^1/_4$-in ID alumina tube was inserted into the molten-salt and then 50 sccm 10 vol% CO_2 (balance Ar) was injected through the tube. The product gas from the outlet was directed to the mass spectrometer downstream (MKS Cirrus 2 by Micromeritics). Inside the $^1/_4$-in ID tube, an additional K-type thermocouple was installed to measure the central temperature of the molten-salt. The measured temperature was

Figure 7. Aspen Plus modeling results

(A) Energy consumptions for MM-ODH and conventional CO_2-ODH, normalized to per metric ton of CO_2 captured and converted.[20]

(B) Process energy requirement for CO_2-ODH with OMS-2 and MM-ODH. The energy requirement for C_2H_4 production and H_2 production were assumed to be 9.9 GJ/ton C_2H_4 (based on stream cracking)[25] and 100 GJ/ton H_2 (based on steam methane reforming).[59]

recorded as the actual reaction temperature. After the measured temperature reached the desired value, 50 sccm 10 vol% CO_2 (balance Ar) was injected from the inner tube for 30 min for carbonate saturation. After that, the excessive gaseous CO_2 was purged with 50 sccm Ar until the CO_2 signal (m/z = 44) in the mass spectrometer reached a steady value. It was noted that due to the constant decomposition of carbonate, this steady CO_2 signal in the mass spectrometer should be above 0. The chemical looping concept of the MM-ODH was demonstrated in a cyclic mode with an ODH step and a subsequent CO_2 capture step. For the ODH step, a 50-sccm 10 vol% ethane (balance Ar) was injected for 4 min, followed by a 50-sccm Ar gas purging for 10 min. A gas bag was used to collect the gas during the entirety of the ethane injection and an additional 4 min of the gas purging (for a total of 8 min). For the CO_2 capture step, a 50-sccm 10 vol% CO_2 (balance Ar) was injected for 20 min to ensure carbonate saturation. The composition of the gas mixture collected by the gas bag would be determined by gas chromatography (Agilent GC 7890 A). The detailed calculation method was detailed in Note S1.2. Other experiments were detailed in Notes S1.3–S1.5.

Thermogravimetric analysis for CO_2 conversion

A TA Instruments SDT Q600 was used to analyze the CO_2 sorption capability of the molten carbonates. The detailed experimental method is described in Notes S1.6 and S1.7.

DRIFTS experiment

Nicolet iS50 Fourier transform infrared (FTIR) spectroscopy was used to analyze the active species in the molten carbonate. The detailed experimental method is described in Note S1.8.

Equilibrium analysis, Aspen Plus Simulation, and AIMD simulations

Outotec HSC 10 was used to calculate the equilibrium component of the reactions. H_2 and Li_2CO_3 (1:50 molar ratio) were used as the initial mixture to calculate the equilibrium products composition (Figure S7). Further details are presented in Note S2.

Aspen Plus simulation (Figure S9A) was used to estimate the energy requirement for MM-ODH. Basic simulation assumptions are listed in Table S4. In the MM-ODH scheme (Figure S8A), the ethane would be fed into the MM reactor and the flue gas would be fed into the regenerator. The depleted Li_2CO_3 would be fed into the regenerator to capture CO_2, and the saturated Li_2CO_3 would be transported into the MM-ODH reactor. The resulting CO and ethylene would be separated via distillation.

In the CO_2-ODH scheme (Figure S8B), the ethane and pre-captured CO_2 was fed into the reactor containing OMS-2. The resulting value-added CO and ethylene were separated via distillation. The energy for each unit was tabulated in Table S5 and the reaction result was tabulated in Table S6.

Ab initio, constant temperature, molecular dynamics (AIMD) simulations were carried out using the Vienna *Ab initio* Simulation Package (VASP). The computation details are provided in Note S4.

SUPPLEMENTAL INFORMATION

Supplemental information can be found online at https://doi.org/10.1016/j.xcrp.2021.100503.

ACKNOWLEDGMENTS

This work was supported by the US Department of Energy (FE0031918), the US National Science Foundation (award no. CBET-1923468), and the Kenan Institute for Engineering, Technology, and Science at NC State University. The authors acknowledge the assistance of Mr. Michael Mantini in helping to construct the molten-salt reactor at North Carolina State University.

AUTHOR CONTRIBUTIONS

J.L. performed the experiments, thermodynamic calculations, and Aspen Plus simulations and wrote the manuscript. F.L. conceived and supervised the project. Y.G. provided guidance and feedback about the manuscript. X.W. performed AIMD simulations.

DECLARATION OF INTERESTS

The authors declare no competing interests.

Received: April 9, 2021
Revised: May 21, 2021
Accepted: June 21, 2021
Published: July 14, 2021

REFERENCES

1. US Energy Information Administration (2019). EIA projects global energy-related CO2 emissions will increase through 2050. https://www.eia.gov/todayinenergy/detail.php?id=41493.

2. Rochelle, G.T. (2009). Amine scrubbing for CO2 capture. Science *325*, 1652–1654.

3. Vitillo, J.G., Smit, B., and Gagliardi, L. (2017). Introduction: Carbon Capture and Separation. Chem. Rev. *117*, 9521–9523.

4. Liang, L., Liu, C., Jiang, F., Chen, Q., Zhang, L., Xue, H., Jiang, H.-L., Qian, J., Yuan, D., and Hong, M. (2017). Carbon dioxide capture and conversion by an acid-base resistant metal-organic framework. Nat. Commun. *8*, 1233.

5. Leung, D.Y.C., Caramanna, G., and Maroto-Valer, M.M. (2014). An overview of current status of carbon dioxide capture and storage technologies. Renew. Sustain. Energy Rev. *39*, 426–443.

6. Zhang, X., Singh, B., He, X., Gundersen, T., Deng, L., and Zhang, S. (2014). Post-combustion carbon capture technologies: Energetic analysis and life cycle assessment. Int. J. Greenh. Gas Control *27*, 289–298.

7. Raynal, L., Alix, P., Bouillon, P.-A., Gomez, A., de Nailly, M., Jacquin, M., Kittel, J., di Lella, A., Mougin, P., and Trapy, J. (2011). The DMX™ process: an original solution for lowering the cost of post-combustion carbon capture. Energy Procedia *4*, 779–786.

8. Pirngruber, G.D., Guillou, F., Gomez, A., and Clausse, M. (2013). A theoretical analysis of the energy consumption of post-combustion CO2 capture processes by temperature swing adsorption using solid sorbents. Int. J. Greenh. Gas Control *14*, 74–83.

9. Bounaceur, R., Lape, N., Roizard, D., Vallieres, C., and Favre, E. (2006). Membrane processes for post-combustion carbon dioxide capture: a parametric study. Energy *31*, 2556–2570.

10. Erlach, B., Schmidt, M., and Tsatsaronis, G. (2011). Comparison of carbon capture IGCC with pre-combustion decarbonisation and with chemical-looping combustion. Energy *36*, 3804–3815.

11. Hepburn, C., Adlen, E., Beddington, J., Carter, E.A., Fuss, S., Mac Dowell, N., Minx, J.C., Smith, P., and Williams, C.K. (2019). The technological and economic prospects for CO_2 utilization and removal. Nature *575*, 87–97.

12. Zimmermann, A.W., Wunderlich, J., Müller, L., Buchner, G.A., Marxen, A., Michailos, S., Armstrong, K., Naims, H., McCord, S., Styring, P., et al. (2020). Techno-Economic Assessment Guidelines for CO2 Utilization. Front. Energy Res. *8*, 5.

13. Yaashikaa, P.R., Senthil Kumar, P., Varjani, S.J., and Saravanan, A. (2019). A review on photochemical, biochemical and electrochemical transformation of CO2 into value-added products. J. CO2 Utilization *33*, 131–147.

14. Gomez, E., Yan, B., Kattel, S., and Chen, J.G. (2019). Carbon dioxide reduction in tandem with light-alkane dehydrogenation. Nat. Rev. Chem. *3*, 638–649.

15. Kuuskraa, V.A., Godec, M.L., and Dipietro, P. (2013). CO2 Utilization from "Next Generation" CO2 Enhanced Oil Recovery Technology. Energy Procedia *37*, 6854–6866.

16. Rahmani, F., Haghighi, M., and Amini, M. (2015). The beneficial utilization of natural zeolite in preparation of Cr/clinoptilolite nanocatalyst used in CO2-oxidative dehydrogenation of ethane to ethylene. J. Ind. Eng. Chem. *31*, 142–155.

17. Baidya, T., van Vegten, N., and Baiker, A. (2011). Selective Conversion of Ethane to Ethene via Oxidative Dehydrogenation Over Ca-doped ThO2 Using CO2 as Oxidant. Top. Catal. *54*, 881–887.

18. Valenzuela, R.X., Bueno, G., Cortés Corberán, V., Xu, Y., and Chen, C. (2000). Selective oxidehydrogenation of ethane with CO2 over CeO2-based catalysts. Catal. Today *61*, 43–48.

19. Zhu, J., Qin, S., Ren, S., Peng, X., Tong, D., and Hu, C. (2009). Na2WO4/Mn/SiO2 catalyst for oxidative dehydrogenation of ethane using CO2 as oxidant. Catal. Today *148*, 310–315.

20. Jin, L., Reutenauer, J., Opembe, N., Lai, M., Martenak, D., Han, S., and Suib, S. (2009). Studies on Dehydrogenation of Ethane in the Presence of CO_2 over Octahedral Molecular Sieve (OMS-2) Catalysts. ChemCatChem *1*, 441–444.

21. Wang, S., Murata, K., Hayakawa, T., Hamakawa, S., and Suzuki, K. (1999). Oxidative dehydrogenation of ethane by carbon dioxide over sulfate-modified Cr2O3/SiO2 catalysts. Catal. Lett. *63*, 59–64.

22. Zhao, X., and Wang, X. (2006). Oxidative dehydrogenation of ethane to ethylene by carbon dioxide over Cr/TS-1 catalysts. Catal. Commun. *7*, 633–638.

23. Gaab, S., Machli, M., Find, J., Grasselli, R.K., and Lercher, J.A. (2008). Oxidative dehydrogenation of ethane over novel Li/Dy/Mg mixed oxides: structure–activity study. Top. Catal. *23*, 151–158.

24. Krylov, O.V., Mamedov, A.Kh., and Mirzabekova, S.R. (1995). The regularities in the

interaction of alkanes with CO2 on oxide catalysts. Catal. Today *24*, 371–375.

25. Haribal, V.P., Neal, L.M., and Li, F. (2017). Oxidative dehydrogenation of ethane under a cyclic redox scheme – process simulations and analysis. Energy *119*, 1024–1035.

26. Wang, Q., Chen, X., Jha, A.N., and Rogers, H. (2014). Natural gas from shale formation – the evolution, evidences and challenges of shale gas revolution in United States. Renew. Sustain. Energy Rev. *30*, 1–28.

27. Ciferno, J. (2020). Developing Technologies for Upcycling Associated Gas into Higher-Value Products. https://www.netl.doe.gov/sites/default/files/2020-12/Upcycling-Associated-Gas-into-Higher-Value-Products-12-2020.pdf.

28. Gärtner, C.A., van Veen, A.C., and Lercher, J.A. (2013). Oxidative Dehydrogenation of Ethane: Common Principles and Mechanistic Aspects. ChemCatChem *5*, 3196–3217.

29. Ranjan, P., Kannan, P., Al Shoaibi, A., and Srinivasakannan, C. (2012). Modeling of Ethane Thermal Cracking Kinetics in a Pyrocracker. Chem. Eng. Technol. *35*, 1093–1097.

30. Sundaram, K.M., and Froment, G.F. (1977). Modeling of thermal cracking kinetics—I. Chem. Eng. Sci. *32*, 601–608.

31. Sundaram, K.M., Van Damme, P.S., and Froment, G.F. (1981). Coke deposition in the thermal cracking of ethane. AIChE J. *27*, 946–951.

32. Van Geem, K.M., Reyniers, M.-F., Marin, G.B., Song, J., Green, W.H., and Matheu, D.M. (2006). Automatic reaction network generation using RMG for steam cracking of n-hexane. AIChE J. *52*, 718–730.

33. Venkataraman, K., Redenius, J.M., and Schmidt, L.D. (2002). Millisecond catalytic wall reactors: dehydrogenation of ethane. Chem. Eng. Sci. *57*, 2335–2343.

34. Deng, S., Li, H., Li, S., and Zhang, Y. (2007). Activity and characterization of modified Cr2O3/ZrO2 nano-composite catalysts for oxidative dehydrogenation of ethane to ethylene with CO2. J. Mol. Catal. Chem. *268*, 169–175.

35. Liu, J., He, N., Zhang, Z., Yang, J., Jiang, X., Zhang, Z., Su, J., Shu, M., Si, R., Xiong, G., et al. (2021). Highly-Dispersed Zinc Species on Zeolites for the Continuous and Selective Dehydrogenation of Ethane with CO_2 as a Soft Oxidant. ACS Catal. *11*, 2819–2830.

36. Zhang, X., Ye, Q., Xu, B., and He, D. (2007). Oxidative dehydrogenation of ethane over Co–BaCO3 catalysts using CO2 as oxidant: effects of Co promoter. Catal. Lett. *117*, 140–145.

37. Yan, B., Yao, S., and Chen, J.G. (2020). Effect of Oxide Support on Catalytic Performance of FeNi-based Catalysts for CO_2 -assisted Oxidative Dehydrogenation of Ethane. ChemCatChem *12*, 494–503.

38. Yan, B., Yao, S., Kattel, S., Wu, Q., Xie, Z., Gomez, E., Liu, P., Su, D., and Chen, J.G. (2018). Active sites for tandem reactions of CO_2 reduction and ethane dehydrogenation. Proc. Natl. Acad. Sci. USA *115*, 8278–8283.

39. Porosoff, M.D., Myint, M.N.Z., Kattel, S., Xie, Z., Gomez, E., Liu, P., and Chen, J.G. (2015). Identifying Different Types of Catalysts for CO_2 Reduction by Ethane through Dry Reforming and Oxidative Dehydrogenation. Angew. Chem. *127*, 15721–15725.

40. Yao, S., Yan, B., Jiang, Z., Liu, Z., Wu, Q., Lee, J.H., and Chen, J.G. (2018). Combining CO2 Reduction with Ethane Oxidative Dehydrogenation by Oxygen-Modification of Molybdenum Carbide. ACS Catal. *8*, 5374–5381.

41. Tian, S., Yan, F., Zhang, Z., and Jiang, J. (2019). Calcium-looping reforming of methane realizes in situ CO_2 utilization with improved energy efficiency. Sci. Adv. *5*, eaav5077.

42. Buelens, L.C., Galvita, V.V., Poelman, H., Detavernier, C., and Marin, G.B. (2016). Super-dry reforming of methane intensifies CO2 utilization via Le Chatelier's principle. Science *354*, 449–452.

43. Al-Mamoori, A., Lawson, S., Rownaghi, A.A., and Rezaei, F. (2020). Oxidative dehydrogenation of ethane to ethylene in an integrated CO2 capture-utilization process. Appl. Catal. B *278*, 119329.

44. Bui, M., Adjiman, C.S., Bardow, A., Anthony, E.J., Boston, A., Brown, S., Fennell, P.S., Fuss, S., Galindo, A., Hackett, L.A., et al. (2018). Carbon capture and storage (CCS): the way forward. Energy Environ. Sci. *11*, 1062–1176.

45. Gupta, H., Lyer, M.V., Sakadjian, B.B., and Fan, L.-S. (2004). Reactive separation of CO2 using pressure pelletised limestone. Int. J. Environ. Technol. Manag. *4*, 3–20.

46. Sakadjian, B.B., Iyer, M.V., Gupta, H., and Fan, L.-S. (2007). Kinetics and Structural Characterization of Calcium-Based Sorbents Calcined under Subatmospheric Conditions for the High-Temperature CO_2 Capture Process. Ind. Eng. Chem. Res. *46*, 35–42.

47. Reisman, A. (1958). Heterogeneous Equilibria in the System K2CO3-Na2CO3. J. Am. Chem. Soc. *81*, 807–811.

48. Kim, S.M., Kierzkowska, A.M., Broda, M., and Müller, C.R. (2017). Sol-gel Synthesis of MgAl2O4-stabilized CaO for CO2 Capture. Energy Procedia *114*, 220–229.

49. Chen, J., Duan, L., and Sun, Z. (2019). Accurate Control of Cage-Like CaO Hollow Microspheres for Enhanced CO_2 Capture in Calcium Looping via a Template-Assisted Synthesis Approach. Environ. Sci. Technol. *53*, 2249–2259.

50. Naeem, M.A., Armutlulu, A., Imtiaz, Q., Donat, F., Schäublin, R., Kierzkowska, A., and Müller, C.R. (2018). Optimization of the structural characteristics of CaO and its effective stabilization yield high-capacity CO_2 sorbents. Nat. Commun. *9*, 2408.

51. Manovic, V., Charland, J.-P., Blamey, J., Fennell, P.S., Lu, D.Y., and Anthony, E.J. (2009). Influence of calcination conditions on carrying capacity of CaO-based sorbent in CO2 looping cycles. Fuel *88*, 1893–1900.

52. MacDowell, N., Florin, N., Buchard, A., Hallett, J., Galindo, A., Jackson, G., Adjiman, C.S., Williams, C.K., Shah, N., and Fennell, P. (2010). An overview of CO2 capture technologies. Energy Environ. Sci. *3*, 1645.

53. Kurlov, A., Armutlulu, A., Donat, F., Studart, A.R., and Müller, C.R. (2020). CaO-Based CO_2 Sorbents with a Hierarchical Porous Structure Made via Microfluidic Droplet Templating. Ind. Eng. Chem. Res. *59*, 7182–7188.

54. Broda, M., and Müller, C.R. (2012). Synthesis of highly efficient, Ca-based, Al_2O_3-stabilized, carbon gel-templated CO_2 sorbents. Adv. Mater. *24*, 3059–3064.

55. Su, C., Duan, L., and Anthony, E.J. (2018). CO2 capture and attrition performance of competitive eco-friendly calcium-based pellets in fluidized bed. Greenhouse Gas Sci Technol. *8*, 1124–1133.

56. Ma, X., Li, Y., Duan, L., Anthony, E., and Liu, H. (2018). CO2 capture performance of calcium-based synthetic sorbent with hollow core-shell structure under calcium looping conditions. Appl. Energy *225*, 402–412.

57. Erans, M., Manovic, V., and Anthony, E.J. (2016). Calcium looping sorbents for CO2 capture. Appl. Energy *180*, 722–742.

58. Janz, G.J. (1967). Molten carbonate electrolytes as acid-base solvent systems. J. Chem. Educ. *44*, 581.

59. Raissi, A.T., and Block, D.L. (2004). Hydrogen: Automotive fuel of the future. IEEE Power Energy Mag. *2*, 40–45.

60. Cassir, M. (1993). Stability and Characterization of Oxygen Species in Alkali Molten Carbonate: A Thermodynamic and Electrochemical Approach. J. Electrochem. Soc. *140*, 3114.